JAIST Repository
https://dspace.jaist.ac.jp/

Title	Interfacial Charge Transfer and Charge Generation in Organic Electronic Devices
Author(s)	Matsushima, Toshinori; Jin, Guang-He; Kanai, Yoshihiro; Yokota, Tomoyuki; Kitada, Seiki; Kishi, Toshiyuki; Murata, Hideyuki
Citation	Organic Electronics, 12(3): 520-528
Issue Date	2011-01-13
Type	Journal Article
Text version	author
URL	http://hdl.handle.net/10119/9826
Rights	NOTICE: This is the author's version of a work accepted for publication by Elsevier. Toshinori Matsushima, Guang-He Jin, Yoshihiro Kanai, Tomoyuki Yokota, Seiki Kitada, Toshiyuki Kishi, and Hideyuki Murata, Organic Electronics, 12(3), 2011, 520-528, http://dx.doi.org/10.1016/j.orgel.2011.01.001
Description	

JAIST
JAPAN
ADVANCED INSTITUTE OF
SCIENCE AND TECHNOLOGY

Japan Advanced Institute of Science and Technology

Interfacial charge transfer and charge generation in organic electronic devices

Toshinori Matsushima, Guang-He Jin, Yoshihiro Kanai, Tomoyuki Yokota, Seiki Kitada,

Toshiyuki Kishi, and Hideyuki Murata*

School of Materials Science, Japan Advanced Institute of Science and Technology, 1-1

Asahidai, Nomi, Ishikawa 923-1292, Japan

ABSTRACT

We have recently proposed that improvement of device performance using a buffer layer of molybdenum trioxide (MoO_3) originates from interfacial charge generation at an interface of MoO_3 and an organic hole-transport layer [Appl. Phys. Lett. 95 (2009) 203306.]. However, there is no clear experimental evidence enough to support the charge generation in our recent report. In this study, from comparison of current density-voltage characteristics of organic hole-only devices and ultraviolet/visible/near-infrared absorption spectra of composite films, we can conclude that the interfacial charge generation surly occurs to

realize space-charge-limited currents of a wide variety of organic hole-transport layers. Moreover, a drastic increase in current density of a bilayer device of *n*-type C60 and *p*-type *N*,*N*´-diphenyl-*N*,*N*´-bis(1-naphthyl)-1,1´-biphenyl-4,4´-diamine (α-NPD) by using a MoO_3 layer can provide the evidence of the charge generation.

* Corresponding author. Tel.: +81 761 51 1531; fax: +81 761 51 1149

E-mail address: murata-h@jaist.ac.jp (H. Murata)

Keywords:

Organic light-emitting diodes

Hole-only devices

Interfacial charge transfer and generation

Organic hole-transport materials and layers

Molybdenum trioxide

1. Introduction

Large charge injection barriers are frequently present at electrode/organic heterojunction interfaces in organic electronic devices, making precisely clarifying charge transport mechanisms of organic thin films difficult because observed current density-voltage (*J*-*V*) characteristics are controlled by both charge injection and transport processes [1-3]. Also, the charge injection barriers are problematic for overall performance of organic electronic devices [4,5]. To solve the injection barrier problem, transition metal oxide, molybdenum trioxide (MoO_3) has been used as a buffer layer between a metal electrode and an organic layer in organic electronic devices, such as organic light-emitting diodes (OLEDs) [6,7], organic solar cells [8,9], and organic thin-film transistors [10,11]. Previously, we have demonstrated that use of a MoO_3 buffer layer with a specific thickness of 0.75 nm between an anode layer of indium tin oxide (ITO) and a hole-transport layer (HTL) of *N*,*N*´-diphenyl-*N*,*N*´-bis(1-naphthyl)-1,1´-biphenyl-4,4´-diamine (α-NPD) leads to an increase in current density by about four orders of magnitude and appearance of a space-charge-limited current (SCLC) of α-NPD [12], indicating that the injection barrier at the ITO/α-NPD interface is completely negligible. This specific MoO_3 thickness of 0.75 nm

is much smaller than those previously used for OLEDs. Power consumption and operational lifetimes of OLEDs are markedly improved by using the 0.75 nm MoO_3 buffer layer as well [5]. Thus, the very thin MoO_3 buffer layer is useful for establishing fundamental physics of charge transport in organic films and for developing the organic electronic devices.

Electronic states of multilayer films and composite films of organic and MoO_3 have been intensively investigated using ultraviolet photoelectron spectroscopy, inverse photoelectron spectroscopy, and X-ray photoelectron spectroscopy [13-16]. These leading papers have shown that: (1) charge transfer between electrode/MoO_3/organic interfaces induces large vacuum level shifts, minimizing a hole injection barrier height, (2) gap states are generated inside band gaps of α-NPD and MoO_3, and (3) a vacuum-deposited MoO_3 layer works as an electron conductor due to donating electrons from gap states to a conduction band. We have recently proposed that the improved device characteristics originate from interfacial charge generation at a MoO_3/HTL interface [17]. However, there is no clear experimental evidence enough to support the charge generation in our recent report. In this study, from comparison of *J-V* characteristics of organic hole-only devices

and ultraviolet/visible/near-infrared (UV-VIS-NIR) absorption spectra of composite films, we can conclude that the interfacial charge generation surly occurs to realize SCLCs of a wide variety of organic HTLs. Moreover, a drastic increase in current density of a bilayer device of *n*-type C60 and *p*-type α-NPD by using a MoO_3 layer can provide the evidence of the charge generation.

The interfacial charge generation mechanism we have recently proposed [17] is composed of (i) electron transfer from a lower-ionization-energy HTL to a higher-work-function MoO_3 layer to form electron-hole pairs at the MoO_3/HTL interface, (ii) separation of the electron-hole pairs under an external electric field, (iii) transit of resultant electrons and holes to corresponding electrodes through a conduction band (or gap states) of MoO_3 and a hole-transport level of α-NPD, and repetition of the charge transfer (i), the charge separation (ii), and the charge transit (iii) for steady-state current flow (Fig. 1). For a well-known standard hole injection mechanism without a MoO_3 buffer layer, HTL-to-ITO electron extraction (transfer) under a local high electric field and separation of electron-hole pairs are repeated in a manner almost similar to the charge generation

mechanism mentioned above [15]. The difference between the charge generation and the charge injection is whether the charge transfer occurs or not under no electric field condition. Using the charge generation mechanism, a well-known charge injection barrier is no longer considered important and *J*-*V* characteristics are controlled by a SCLC. Since the HTL-to-MoO_3 electron transfer characteristics are expected to be related to a difference between an ionization energy of an HTL and a work function of a MoO_3 layer, a relationship between *J*-*V* characteristics and electron transfer characteristics is investigated in this study when ionization energies of HTL materials are systematically changed (see Fig. 2).

2. Experimental

HTL materials used in this study are 4,4′,4′′-tris(*N*-3-methylphenyl-*N*-phenyl-amino)triphenylamine (m-MTDATA), *fac*-tris(2-phenylpyridinato)iridium(III) [$Ir(ppy)_3$], 4,4′,4′′-tris(*N*-2-naphthyl-*N*-phenyl-amino)triphenylamine (2-TNATA), *N*,*N*′-di(m-tolyl)-*N*,*N*′-diphenylbenzidine (TPD), rubrene, α-NPD, 2,4,6-tricarbazolo-1,3,5-triazine (TRZ-2), and 4,4′-bis(carbazol-9-yl)-2,2′-biphenyl (CBP)

(the chemical structures of the HTL molecules are shown in Fig. 2). Hole-only device structures and bilayer device structures of C60 and α-NPD are glass substrate/ITO anode (150 nm)/MoO_3 buffer layer (*X* nm)/m-MTDATA, $Ir(ppy)_3$, 2-TNATA, TPD, rubrene, α-NPD, TRZ-2, or CBP HTL (100 nm)/MoO_3 electron-blocking layer (EBL) (10nm)/Al cathode (100 nm) and glass substrate/ITO anode (150 nm)/*n*-type C60 layer (30 nm)/MoO_3 buffer layer (0 or 5 nm)/*p*-type α-NPD HTL (100 nm)/MoO_3 EBL (10 nm)/Al cathode (100 nm), respectively. Source materials of m-MTDATA (Luminescence Technology), 2-TNATA (Luminescence Technology), rubrene (Aldrich), TRZ-2 (Luminescence Technology), and C60 (Materials Technologies Research) were purchased and purified twice using a vacuum train sublimation technique prior to evaporation. High-purity source materials of $Ir(ppy)_3$ (Nippon Steel Chemical), TPD (Tokyo Chemical Industry), α-NPD (Nippon Steel Chemical), CBP (Nippon Steel Chemical), MoO_3 (Mitsuwa Chemicals), and Al (Nilaco) were purchased and used as-received. The glass substrates coated with the 150 nm ITO anode layer with a sheet resistance of 10 Ω sq^{-1} (SLR grade) were purchased from Sanyo Vacuum Industries and the ITO layers were patterned by conventional photolithography. The substrates were cleaned using ultrasonication in acetone, followed by ultrasonication in detergent, pure water, and

isopropanol. Then, the substrates were placed in an UV-ozone treatment chamber for 30 min. After the cleaning, the substrates were set in an evaporation chamber. The chamber was evacuated to a base pressure of $\approx 10^{-4}$ Pa. The layers of the MoO_3 and the organic materials were thermally deposited on the ITO surface from an alumina crucible (MoO_3) and individual carbon crucibles (organic materials). To complete the devices, the Al cathode layer was thermally deposited from a tungsten basket through a shadow mask with openings. The deposition rates were precisely controlled at 0.05 nm s^{-1} (MoO_3), 0.1 nm s^{-1} (organic materials), and 0.5 nm s^{-1} (Al) using a calibrated quartz crystal microbalance. The active device area was defined at 4 mm^2 by the overlapped area of the ITO layer and the Al layer. The completed devices were transferred to a nitrogen-filled glove box (O_2 and H_2O levels are less than 2 ppm) without exposing the devices to ambient air and encapsulated using a glass cap and an UV curing epoxy resin together with a desiccant sheet. The steady-state *J-V* characteristics of the devices were measured using a semiconductor characterization system (SCS4200, Keithley) at room temperature when the MoO_3 thicknesses (*X*) and the HTL materials are systematically changed. Since no electroluminescence was observed during the *J-V* measurements, it was confirmed that holes are dominant charge carriers in our devices.

A 50 nm organic layer, a 50 nm MoO_3 layer, and a 50 nm Al layer were thermally deposited on the cleaned ITO substrates using the preparation conditions described above. The ionization energies and the work functions of the layers were measured using an UV photoelectron spectrometer in air (AC-2, Riken Keiki). The work function of ITO was measured from the UV-ozone-treated bare ITO surface using the AC-2. The electron affinities of the organic layers were estimated by subtracting their absorption onset energies from the ionization energies.

Devices with a structure of glass substrate/Al electrode (100 nm)/organic layer (200 nm)/Al layer (100 nm) were fabricated using the preparation conditions described above. To calculate the relative permittivities, the capacitance of the organic layers was measured using an LCR meter (4284A, Agilent). The input voltage and the amplitude of the input signal were set at 0.1 V and ±0.005 V, respectively. No current flow was confirmed under the capacitance measurements. The capacitance of the organic layers remained constant in a frequency range from 20 Hz to 100 kHz.

50 nm intrinsic organic films and 50 nm composite films of organic and MoO_3 were thermally deposited on cleaned quartz substrates. The deposition ratio of organic to MoO_3 was controlled at 1:1 by mol using a calibrated quartz crystal microbalance. The total deposition rate was fixed at ≈0.1 nm s^{-1}. The UV-VIS-NIR absorption spectra of the intrinsic films and the composite films were measured using an absorption spectrometer (V670, JASCO).

3. Results and discussion

3.1. Current density-voltage characteristics

The ionization energies of the HTL materials are measured as summarized in Table 1. The work functions of ITO, MoO_3, and Al are also measured respectively to be 5.02±0.02, 5.68±0.03, and 3.58±0.02 eV. The work function of MoO_3 corresponds to a difference between a vacuum level and a Fermi level right below a conduction band edge [16]. The ionization energies and the work functions we measured here may be slightly different from actual values because they are measured in air [18]. In fact, the work function of a fresh Al

surface has been measured to be ≈4.0 eV in an ultra-high vacuum condition [19]. The corresponding energy-level diagram with these values is shown in Fig. 2.

If an Ohmic contact is formed at an electrode/organic interface and a free charge density is negligible in comparison to an injected charge density, a SCLC with field-dependent mobilities is expressed as the equation [20]:

$$J = \frac{9}{8}\varepsilon_r \varepsilon_0 \mu_0 \exp\left(0.89\beta \frac{V^{0.5}}{L^{0.5}}\right)\left(\frac{V^2}{L^3}\right) \quad (1),$$

where ε_r is the relative permittivity, ε_0 is the vacuum permittivity, μ_0 is the zero field mobility, β is the field dependence parameter, and L is the film thickness. The relative permittivities of the HTLs are determined as summarized in Table 1 by measuring their capacitance. By fitting the obtained *J*-*V* characteristics with the SCLC equation (1), the zero field hole mobilities and the field dependence parameters can be determined at the same time.

The *J*-*V* characteristics of m-MTDATA, $Ir(ppy)_3$, and 2-TNATA are independent of the MoO_3 thicknesses *X* and are well fitted with the SCLC equation (1) (Figs. 3a, 3b, and 3c),

indicating that the *J-V* characteristics are controlled by the SCLCs and the junctions of ITO/m-MTDATA, ITO/Ir(ppy)$_3$, and ITO/2-TNATA are already Ohmic contacts without the MoO_3 buffer layer. We assume that the small barrier heights less than ≈0.1 eV no longer affect the *J-V* characteristics. Indeed, it has been shown that ITO forms ideal hole-injecting contacts with m-MTDATA [21] and 2-TNATA [22], which agree with our results.

On the other hand, the *J-V* characteristics of TPD, rubrene, and α-NPD are markedly dependent upon the MoO_3 thicknesses *X* (Figs. 3d, 3e, and 3f). The current densities at the MoO_3 thickness of 0 nm are very small due to the relatively large hole injection barrier heights ranging from ≈0.2 to ≈0.4 eV. The current densities increase $\approx 10^4$ times and then decrease $\approx 10^1$ times as the MoO_3 thicknesses are increased. Details of the changes in the *J-V* characteristics have been discussed in our recent paper [17]. The optimized MoO_3 thicknesses are 1.0 nm for rubrene and 0.75 nm for TPD and α-NPD, which provide the highest current densities for the devices. Since the electron transfer from these HTLs to the MoO_3 layer can be confirmed (the electron transfer characteristics will be discussed later), the marked increase in current density by using the MoO_3 buffer layer is attributable to the

interfacial charge generation mechanism as illustrated in Fig. 1. The *J-V* characteristics at the optimized thicknesses can be fitted with the SCLC equation (1).

The *J-V* characteristics of TRZ-2 and CBP slightly shift to higher current densities by using the MoO_3 buffer layer maybe due to a reduction in hole injection barrier height caused by the high-work-function MoO_3, but cannot be fitted with the SCLC equation (1) (Figs. 3g and 3h), indicating that the *J-V* characteristics are still controlled by injection-limited currents. Since the ionization energies of TRZ-2 (≈5.68 eV) and CBP (≈5.96 eV) are equal to or higher than the work function of MoO_3 (≈5.68 eV), no charge transfer and no charge generation occur at the HTL/MoO_3 interfaces.

The *J-V* characteristics of the hole-only devices with various HTL thicknesses (*L*) ranging from 50 to 800 nm are investigated (see Fig. 4). The optimized MoO_3 thicknesses (*X*) are used for the devices [0 nm for m-MTDATA, $Ir(ppy)_3$, and 2-TNATA, 0.75 nm for TPD and α-NPD, and 1 nm for rubrene]. The *J-V* characteristics of all the devices can be fitted with the SCLC equation (1) when the field dependence parameters summarized in

Table 1 are used for the SCLC fitting. The zero field hole mobilities estimated from the SCLC regions are plotted versus the HTL thicknesses in Fig. 5. The zero field hole mobilities are found to gradually increase as the thicknesses of the HTLs are increased.

The zero field mobilities and the field dependence parameters estimated from the SCLC regions are compared with those of m-MTDATA [23], 2-TNATA [22], TPD [24], rubrene [25], and α-NPD [24] measured using a time-of-flight (TOF) technique (Table 1). In this Table, we summarize the zero field hole mobilities and the field dependence parameters of the 200 nm HTL layers because the zero field hole mobilities are dependent on the film thicknesses and the mobility of the 100 nm α-NPD HTL does not still reach a saturation value. While the SCLC field dependence parameters are almost similar to the TOF field dependence parameters, the SCLC zero field mobilities are about one order of magnitude lower than the TOF zero field mobilities. It has been shown that electron mobilities of tris(8-hydroxyquinoline)aluminum (Alq_3) [26] and 4,7-diphenyl-1,10-phenanthroline (Bphen) [27] and hole mobilities of α-NPD [3] and 2-TNATA [28] depend on their film

thicknesses. Chu and Song have attributed the thickness-dependent mobilities to a change in hole trap concentration in organic films [3].

While the *J-V* characteristics of TPD, rubrene, and α-NPD are dependent upon the MoO_3 thicknesses, the *J-V* characteristics of m-MTDATA, $Ir(ppy)_3$, and 2-TNATA are independent of the MoO_3 thicknesses as shown in Fig. 3. One possible explanation for the independent and dependent *J-V* characteristics is a difference in hole mobility between the organic layers. The layers of m-MTDATA, $Ir(ppy)_3$, and 2-TNATA have lower hole mobilities than the other layers of TPD, rubrene, and α-NPD have as summarized in Table 1. Thus, the *J-V* characteristics of m-MTDATA, $Ir(ppy)_3$, and 2-TNATA are strongly limited by a bulk hole transport process due to their lower mobilities, thereby obscuring the dependency of the *J-V* characteristics of m-MTDATA, $Ir(ppy)_3$, and 2-TNATA.

Built-in potential (a difference between Fermi levels of an anode and a cathode) sometimes makes difficult to analyze charge injection and transport characteristics of organic electronic devices [29,30]. To investigate whether the built-in potential is present or

not in our devices, the *J-V* characteristics of the hole-only devices with the structures of glass substrate/ITO anode (150 nm)/2-TNATA HTL (100 nm)/MoO_3 EBL (0 or 10 nm)/Al cathode (100 nm) are compared in the forward and reverse bias directions (Fig. 6). The reverse biased ITO/2-TNATA/Al device has much smaller current densities than the other devices have due to large charge injection barriers for both electrons and holes. No current flow is observed in a low voltage region of the forward biased ITO/2-TNATA/Al device due to the presence of the built-in potential. The built-in potential is roughly estimated to be ≈1.0 eV from a difference between the work functions of ITO (5.02±0.02 eV) and Al (≈4.0 eV [19]). However, the estimated value is larger than the observed turn-on voltage (≈0.6 V), perhaps resulting from that actual built-in potential is slightly changed by a vacuum level shift [19].

Otherwise, the *J-V* characteristics of the forward and reverse biased ITO/2-TNATA/MoO_3/Al devices are completely overlapped and well explained with the SCLC equation (1), indicating that the influence of the built-in potential on the *J-V* characteristics is completely negligible by using the MoO_3 EBL. We assume that a Fermi

level of MoO_3 is pinned near a hole-transport level of 2-TNATA due to the electron transfer from the 2-TNATA HTL to the MoO_3 layer, resulting in the completely overlapped *J-V* characteristics in both bias directions.

3.2. Electron transfer characteristics

To confirm the HTL-to-MoO_3 electron transfer under no electric field, the UV-VIS-NIR absorption spectra of the 50 nm intrinsic organic films and the 50 nm composite films of organic:MoO_3 (1:1 by mol) on the quartz substrates are measured (Fig. 7). The absorption peaks appear in the NIR region for the composite films [m-MTDATA, $Ir(ppy)_3$, 2-TNATA, TPD, rubrene, and α-NPD] when compared with their intrinsic films. The NIR peaks are attributable to generation of radical cations of HTL molecules, resulting from the electron transfer [31,32]. On the other hand, there is no absorption peak in the NIR region for the other composite films (TRZ-2 and CBP). These results indicate that the ionization energies of the HTLs must be lower than the work function of MoO_3 to induce the HTL-to-MoO_3 electron transfer.

A reduction in hole injection barrier height by using a MoO_3 buffer layer has been reported by analyzing electronic structures of electrode/MoO_3/organic interfaces using photoelectron spectroscopy [13-16] although it is still difficult to estimate actual hole injection barrier heights under operation of devices. Thus, the standard hole injection mechanism from the ITO anode to the HTL through the MoO_3 layer cannot be ruled out. However, since the electron transfer characteristics (Fig. 7) are in good agreement with the SCLC characteristics (Figs. 3 and 4), the interfacial charge generation mechanism surely occurs in addition to the hole injection mechanism. Since the charge generation rate is found to be high enough to realize the SCLCs (this evidence will be presented in the next section), we are able to conclude that the charge generation is a more dominant mechanism than the hole injection when the MoO_3 buffer layer is used.

The work functions of MoO_3 reported thus far are in a wide range from 5.3 to 6.86 eV [11,12,14-16,33]. Also, CBP-to-MoO_3 electron transfer has been confirmed from photoelectron spectroscopy under an ultra-high vacuum condition [14], which is in contrast to no CBP-to-MoO_3 electron transfer observed here. It has been shown that a major

molecular species vaporizing is polymeric, $(MoO_3)_n$ [15,34] and oxygen vacancy defects are present in the resulting oxide films [16,33,35]. We assume that preparation conditions of the oxide films (such as a deposition rate and a partial pressure of oxygen inside a vacuum evaporator) affect degrees of the clustering and the oxygen vacancy defects, which further affect the work functions and the electron transfer characteristics. It has been shown that the amount of the oxygen vacancy defects are changed by annealing the oxide films in a vacuum [16] and exposing the oxide films to ambient air [35]. Also, Meyer et al. have reported that contamination by air exposure of the oxide film reduces its work function by about 1 eV [36]. We suggest that the charge generation is possible for the higher-ionization-energy materials (such as TRZ-2 and CBP) if the preparation conditions are favorably controlled and/or other higher-work-function metal oxide is used [such as WO_3 (6.4 eV) [37]].

3.3. Interfacial charge generation

To obtain the evidence of the interfacial charge generation, the *J-V* characteristics of two types of the devices are measured and compared [glass substrate/ITO anode (150

nm)/*n*-type C60 layer (30 nm)/MoO_3 buffer layer (0 or 5 nm)/*p*-type α-NPD HTL (100 nm)/MoO_3 EBL (10 nm)/Al cathode (100 nm)] [Fig. 8]. Although it has been reported that a thin C60 layer (2.5 nm) improves hole injection from ITO [3], the use of the thick C60 layer (30 nm) between the ITO layer and the α-NPD layer extremely lowers the current densities of the C60/α-NPD device (Fig. 8a) due to effective blocking of hole injection from the ITO layer to the high-ionization-energy C60 layer (Fig. 8b). Surprisingly, the current densities markedly increase by inserting the MoO_3 layer between the C60 layer and the α-NPD layer. This increase in current density originates from the interfacial charge generation mechanism, which is composed of α-NPD-to-MoO_3 electron transfer to form electron-hole pairs, separation of the electron-hole pairs under an electric field, and transit of electrons and holes to corresponding electrodes through a conduction band (or gap states) of MoO_3, an electron-transport level of C60, and a hole-transport level of α-NPD (see Fig. 8b). A similar phenomenon has been observed in stacked OLEDs with a charge generation layer consisting of alkali metal and transition metal oxide [33,38,39]. Since there is negligible hole injection from the ITO layer for these devices, it is suggested that the charge generation rate is high enough to realize the SCLC. The current densities of the C60/MoO_3/α-NPD device are

slightly lower than a SCLC level observed in the α-NPD device with the optimized MoO_3 thickness [glass substrate/ITO anode (150 nm)/MoO_3 buffer layer (0.75 nm)/α-NPD HTL (100 nm)/MoO_3 EBL (10 nm)/Al cathode (100 nm)]. The lower current densities would be due to the presence of an electron injection barrier at the C60/MoO_3 interface as shown in Fig. 8b.

4. Conclusions

J-V characteristics of organic hole-only devices having a MoO_3 buffer layer and UV-VIS-NIR absorption spectra of composite films of organic and MoO_3 are investigated when HTL materials with different ionization energies are systematically changed. We find that SCLCs of a wide variety of HTLs are observed and their hole mobilities can be estimated using a SCLC analysis when ionization energies of HTLs are lower than a work function of MoO_3. From comparison of the *J-V* characteristics and the UV-VIS-NIR absorption spectra, the HTL-to-MoO_3 electron transfer is crucial to realizing the SCLCs. Thus, we can attribute the observation of the SCLCs by using the MoO_3 buffer layer to an interfacial charge generation mechanism (composed of charge transfer, separation, and

transit as shown in Fig. 1). Finally, we would like to mention that the interfacial charge generation is a versatile technique used to eliminate an influence of hole injection barriers on *J-V* characteristics of organic electronic devices.

Acknowledgement

This work is supported by Grants-in-Aid for Scientific Research (No. 21760005, No. 20241034, and No. 20108012). Part of this work is based on "Development of the next generation large-scale organic electroluminescence display basic technology (Green IT Project)" with New Energy and Industrial Technology Development Organization (NEDO).

References

[1] M. Abkowitz, J. S. Facci, J. Rehm, J. Appl. Phys. 83 (1998) 2670.

[2] G. G. Malliaras, J. C. Scott, J. Appl. Phys. 83 (1998) 5399.

[3] T.-Y. Chu, O.-K. Song, Appl. Phys. Lett. 90 (2007) 203512.

[4] I. D. Parker, J. Appl. Phys. 75 (1994) 1656.

[5] T. Matsushima, G.-H. Jin, H. Murata, J. Appl. Phys. 104 (2008) 054501.

[6] S. Tokito, K. Noda, Y. Taga, J. Phys. D: Appl. Phys. 29 (1996) 2750.

[7] C.-W. Chen, Y.-J. Lu, C.-C. Wu, E. H.-E. Wu, C.-W. Chu, Y. Yang, Appl. Phys. Lett. 87 (2005) 241121.

[8] V. Shrotriya, G. Li, Y. Yao, C.-W. Chu, Y. Yang, Appl. Phys. Lett. 88 (2006) 073508.

[9] Y. Kinoshita, R. Takenaka, H. Murata, Appl. Phys. Lett. 92 (2008) 243309.

[10] G. L. Frey, K. J. Reynolds, R. H. Friend, Adv. Mater. 14 (2002) 265.

[11] C.-W. Chu, S.-H. Li, C.-W. Chen, V. Shrotriya, Y. Yang, Appl. Phys. Lett. 87 (2005) 193508.

[12] T. Matsushima, Y. Kinoshita, H. Murata, Appl. Phys. Lett. 91 (2007) 253504.

[13] H. Lee, S. W. Cho, K. Han, P. E. Jeon, C.-N. Whang, K. Jeong, K. Cho, Y. Yi, Appl. Phys. Lett. 93 (2008) 043308.

[14] M. Kröger, S. Hamwi, J. Meyer, T. Riedl, W. Kowalsky, A. Kahn, Org. Electron. 10 (2009) 932.

[15] M. Kröger, S. Hamwi, J. Meyer, T. Riedl, W. Kowalsky, A. Kahn, Appl. Phys. Lett. 95 (2009) 123301.

[16] K. Kanai, K. Koizumi, S. Ouchi, Y. Tsukamoto, K. Sakanoue, Y. Ouchi, K. Seki, Org. Electron. 11 (2010) 188.

[17] T. Matsushima, H. Murata, Appl. Phys. Lett. 95 (2009) 203306.

[18] Y. Kawamura, H. Sasabe, C. Adachi, Jpn. J. Appl. Phys. 43 (2004) 7729.

[19] H. Ishii, K. Sugiyama, E. Ito, K. Seki, Adv. Mater. 11 (1999) 605.

[20] P. N. Murgatroyd, J. Phys. D: Appl. Phys. 3 (1970) 151.

[21] C. Giebeler, H. Antoniadis, D. D. C. Bradley, Y. Shirota, Appl. Phys. Lett. 72 (1998) 2448.

[22] C. H. Cheung, K. C. Kwok, S. C. Tse, S. K. So, J. Appl. Phys. 103 (2008) 093705.

[23] S. W. Tsang, S. K. So, J. B. Xu, J. Appl. Phys. 99 (2006) 013706.

[24] S. Naka, H. Okada, H. Onnagawa, Y. Yamaguchi, T. Tsutsui, Synth. Met. 111-112 (2000) 331.

[25] H. H. Fong, S. K. So, W. Y. Sham, C. F. Lo, Y. S. Wu, C. H. Chen, Chem. Phys. 298 (2004) 119.

[26] S. C. Tse, H. H. Fong, S. K. So, J. Appl. Phys. 94 (2003) 2033.

[27] W. Xu, Khizar-ul-Haq, Y. Bai, X. Y. Jiang, Z. L. Zhang, Solid State Commun. 146 (2008) 311.

[28] O. J. Weiß, R. K. Krause, A. Hunze, J. Appl. Phys. 103 (2008) 043709.

[29] T. M. Brown, J. S. Kim, R. H. Friend, F. Cacialli, R. Daik, W. J. Feast, Appl. Phys. Lett. 75 (1999) 1679.

[30] T. M. Brown, R. H. Friend, I. S. Milard, D. J. Lacey, T. Butler, J. H. Burroughes, F. Cacialli, J. Appl. Phys. 93 (2003) 6159.

[31] X. Zhou, J. Blochwitz, M. Pfeiffer, A. Nollau, T. Fritz, K. Leo, Adv. Funct. Mater. 11 (2001) 310.

[32] D.-S. Leem, H.-D. Park, J.-W. Kang, J.-H. Lee, J. W. Kim, J.-J. Kim, Appl. Phys. Lett. 91 (2007) 011113.

[33] H. Kanno, N. C. Giebink, Y. Sun, S. R. Forrest, Appl. Phys. Lett. 89 (2006) 023503.

[34] J. Berkowitz, M. G. Inghram, W. A. Chupka, J. Chem. Phys. 26 (1957) 842.

[35] C. H. Cheung, W. J. Song, S. K. So, Org. Electron. 11 (2010) 89.

[36] J. Meyer, A. Shu, M. Kröger, A. Kahn, App. Phys. Lett. 96 (2010) 133308.

[37] J. Meyer, S. Hamwi, T. Bülow, H.-H. Johannes, T. Riedl, W. Kowalsky, Appl. Phys. Lett. 91 (2007) 113506.

[38] T. Tsutsui, M. Terai, Appl. Phys. Lett. 84 (2004) 440.

[39] J. Meyer, M. Kröger, S. Hamwi, F. Gnam, T. Riedl, W. Kowalsky, A. Kahn, Appl. Phys. Lett. 96 (2010) 193302.

Table 1. Ionization energies (IE), relative permittivities (ε_r), zero field hole mobilities (μ_0), and field dependence parameters (β) of HTL materials with the thickness of 200 nm.

HTL material	IE (eV)	ε_r	SCLC		TOF	
			μ_0 [$cm^2 V^{-1} s^{-1}$]	β [$cm^{0.5} V^{-0.5}$]	μ_0 [$cm^2 V^{-1} s^{-1}$]	β [$cm^{0.5} V^{-0.5}$]
m-MTDATA	5.06±0.02	2.76±0.02	$(2.2\pm0.2)\times10^{-6}$	$(4.3\pm0.4)\times10^{-3}$	1.6×10^{-5} [23]	1.8×10^{-3} [23]
$Ir(ppy)_3$	5.11±0.02	3.35±0.05	$(2.2\pm0.2)\times10^{-8}$	$(1.0\pm0.1)\times10^{-2}$	No data reported	
2-TNATA	5.13±0.02	2.77±0.04	$(6.8\pm0.5)\times10^{-6}$	$(3.1\pm0.2)\times10^{-3}$	1.8×10^{-5} [22]	2.0×10^{-3} [22]
TPD	5.24±0.02	3.38±0.03	$(1.4\pm0.1)\times10^{-4}$	$(2.0\pm0.2)\times10^{-3}$	6.6×10^{-4} [24]	1.0×10^{-3} [24]
Rubrene	5.29±0.01	2.78±0.03	$(2.5\pm0.2)\times10^{-4}$	$(1.1\pm0.2)\times10^{-3}$	4.9×10^{-3} [25]	1.8×10^{-3} [25]
α-NPD	5.40±0.01	3.42±0.02	$(3.3\pm0.3)\times10^{-4}$	$(8.0\pm0.6)\times10^{-4}$	4.0×10^{-4} [24]	1.1×10^{-3} [24]
TRZ-2	5.68±0.02	3.24±0.05	No SCLC observed			
CBP	5.96±0.02	2.62±0.03	No SCLC observed			

Figure captions

Fig. 1. Illustrations of energy-level diagrams showing charge generation mechanism, which is composed of (i) charge transfer, (ii) charge separation, and (iii) charge transit. These processes (i), (ii), and (iii) are repeated for steady-state current flow. CBE, VBE, HOMO, and LUMO stand for conduction band edge, valence band edge, highest occupied molecular orbirtal, and lowest unoccupied molecular orbirtal, respectively.

Fig. 2. Chemical structures of organic molecules and energy-level diagrams.

Fig. 3. *J-V* characteristics of hole-only devices, where 100 nm HTL layers are changed from (a) m-MTDATA, (b) $Ir(ppy)_3$, (c) 2-TNATA, (d) TPD, (e) rubrene, (f) α-NPD, (g) TRZ-2, and (h) CBP and MoO_3 thicknesses (*X*) are changed from 0 to 10 nm. Solid lines represent SCLCs.

Fig. 4. *J-V* characteristics of hole-only devices with structures of glass substrate/ITO anode (150 nm)/MoO_3 buffer layer (*X* nm)/(a) m-MTDATA, (b) $Ir(ppy)_3$, (c) 2-TNATA, (d) TPD, (e) rubrene, or (f) α-NPD HTL (*L* nm)/MoO_3 EBL (10nm)/Al cathode (100 nm). HTL thicknesses (*L*) are changed in range from 50 to 800 nm. Optimized MoO_3 thicknesses (*X*) are used [0 nm for m-MTDATA, $Ir(ppy)_3$, and 2-TNATA, 0.75 nm for TPD and α-NPD, and 1 nm for rubrene]. Solid lines represent SCLCs. Field dependence parameters (β) summarized in Table 1 are used for SCLC fitting. Estimated zero field hole mobilities are shown in Fig. 5.

Fig. 5. Zero field hole mobility (μ_0)-film thickness (*L*) characteristics of (a) m-MTDATA, (b) $Ir(ppy)_3$, (c) 2-TNATA, (d) TPD, (e) rubrene, and (f) α-NPD. Zero field hole mobilities of HTLs are estimated by fitting *J-V* characteristics shown in Fig. 4 with SCLC equation (1).

Fig. 6. *J-V* characteristics of 2-TNATA hole-only devices in forward and reverse bias directions. Solid line represents SCLC.

Fig. 7. UV-VIS-NIR absorption spectra of intrinsic organic films and composite films of organic and MoO_3 (1:1 by mol).

Fig. 8. (a) *J-V* characteristics of devices based on C60 and α-NPD. Solid line represents SCLC. (b) Energy-level diagrams showing charge generation mechanism of this device. Electron injection barrier at C60/MoO_3 interface is roughly estimated to be ≈0.79 eV from difference between electron affinity of C60 (≈4.89 eV) and work function of MoO_3 (≈5.68 eV).

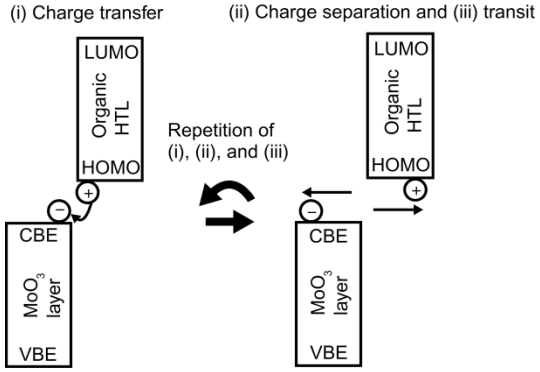

Fig. 1.

Matsushima *et al.*

Organic Electronics

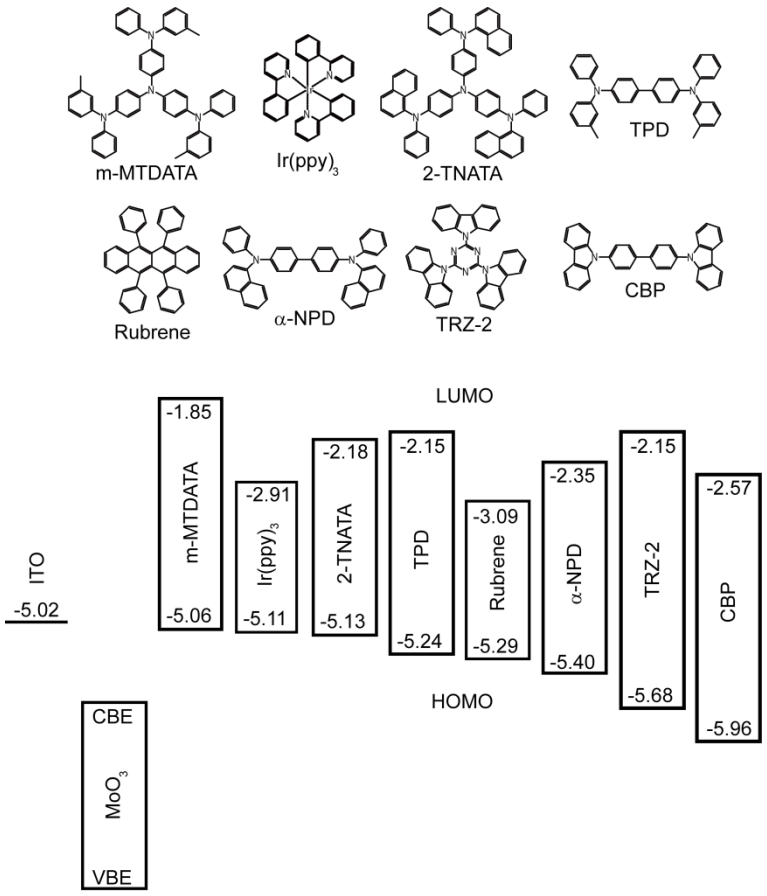

Fig. 2.

Matsushima *et al*.

Organic Electronics

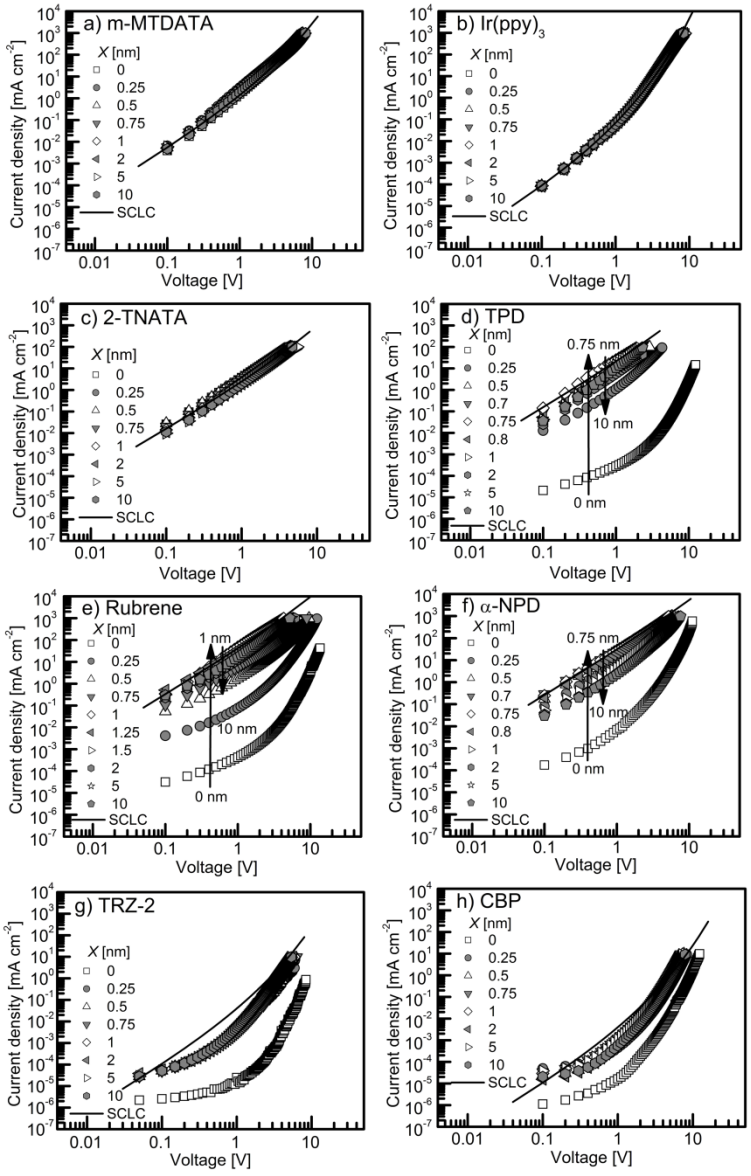

Fig. 3.

Matsushima *et al*.

Organic Electronics

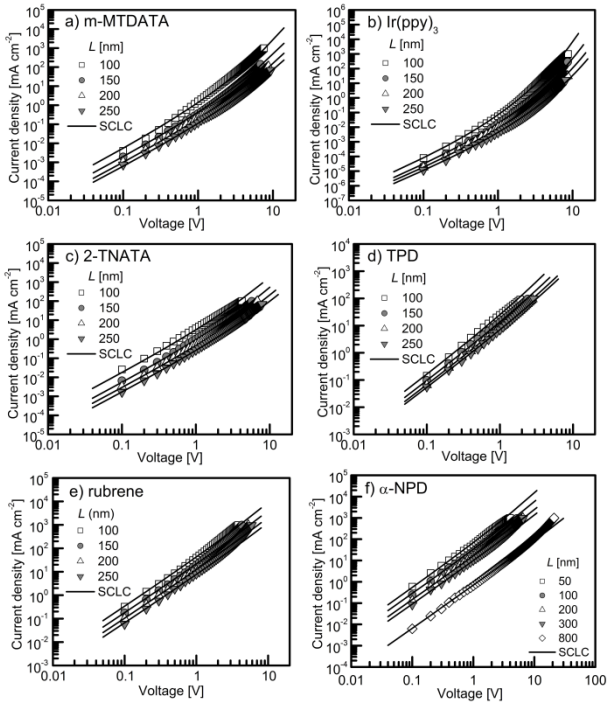

Fig. 4.

Matsushima *et al*.

Organic Electronics

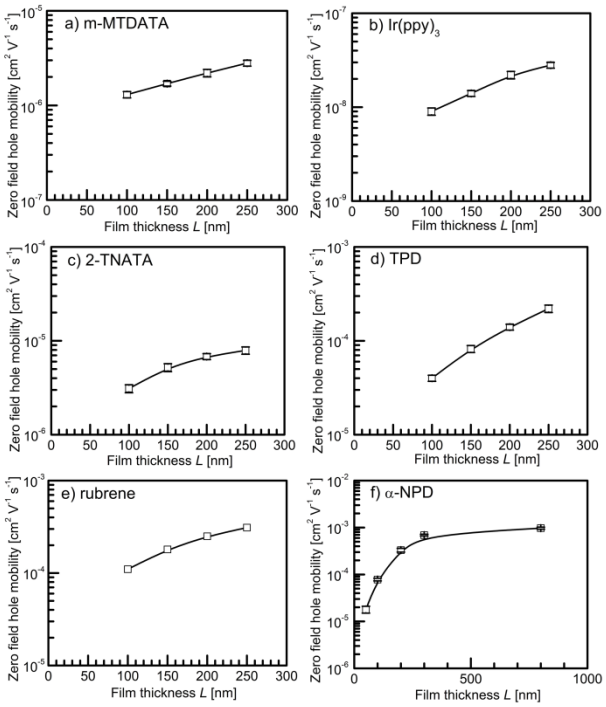

Fig. 5.

Matsushima *et al*.

Organic Electronics

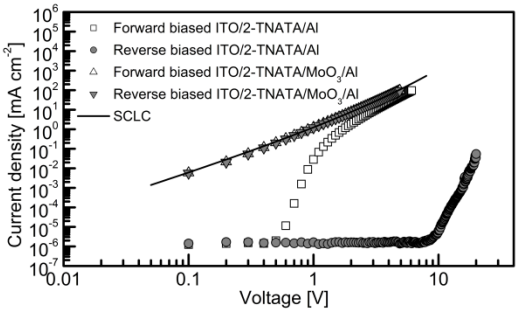

Fig. 6.

Matsushima *et al*.

Organic Electronics

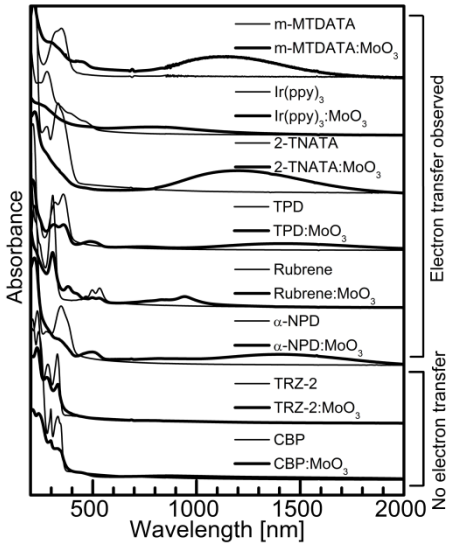

Fig. 7.

Matsushima *et al*.

Organic Electronics

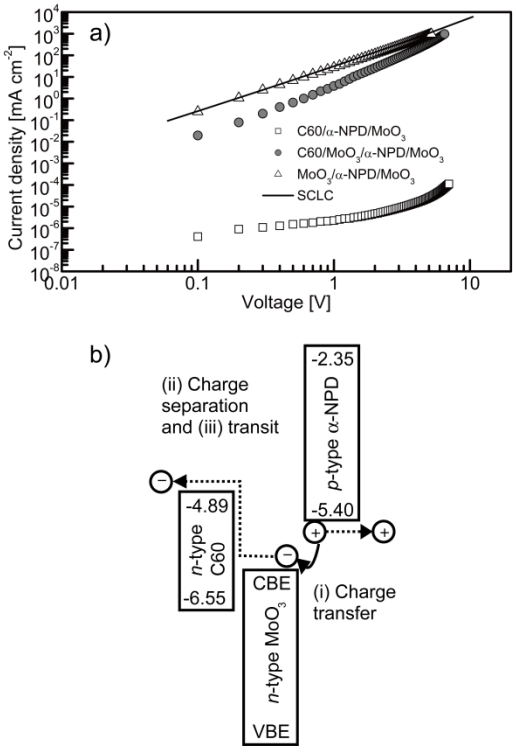

Fig. 8.

Matsushima *et al.*

Organic Electronics